On Combining Visual SLAM and Visual Odometry

Brian Williams and Ian Reid

Abstract— **Sequential monocular SLAM systems perform drift free tracking of the pose of a camera relative to a jointly estimated map of landmarks. To allow real-time operation in moderately sized environments, the map is kept quite spare with usually only tens of landmarks visible in each frame. In contrast, visual odometry techniques track hundreds of visual features per frame. This leads to a very accurate estimate of the relative camera motion, but without a persistent map, the estimate tends to drift over time. We demonstrate a new monocular SLAM system which combines the benefits of these two techniques. In addition to maintaining a sparse map of landmarks in the world, our system finds as many inter-frame point matches as possible. These point matches provide additional constraints on the inter-frame motion of the camera leading to a more accurate pose estimate, and, since they are not maintained as full map landmarks, they do not cause a large increase in the computational cost. Our results in both a simulated environment and in real video demonstrate the improvement in estimation accuracy gained by the inclusion of visual odometry style observations. The constraints available from pairwise point matches are most naturally cast in the context of a camera-centric rather than world-centric frame. To that end we recast the usual world-centric EKF implementation of visual SLAM in a robo-centric frame. We show that this robo-centric visual SLAM, as expected, leads to the estimated uncertainty more closely matching the ideal uncertainty; i.e., that robo-centric visual SLAM yields a more consistent estimate than the traditional world-centric EKF algorithm.**

I. INTRODUCTION

As a camera moves through its environment, the motion of image features can be used to determine the trajectory of the camera and the three dimensional structure of the scene. Though the boundary is somewhat arbitrary, generally speaking, if the algorithm for estimating the trajectory works by matching features between image frames, it is classed as preforming "visual odometry", while if the matching is between a live map of the scene structure and the current image, it is classed as "visual SLAM".

A significant advantage of the latter is that repeated observation of the same features ensures that the trajectory estimate does not drift over time. Furthermore, though in monocular visual SLAM the scale is arbitrary, once set it is fixed by the map. The price of this, however, is the cost of building and maintaining the map. Current visual SLAM systems based on the EKF, say, (such as [1]) are limited in the size of the map by the computational complexity of maintaining the coupled pose and scene covariance. This in turn limits the number of feature matches available at any instant to those map features which project to the current view. This may be only a few, and occasionally too few to fully constrain the pose.

In contrast, a visual odometry system based on two-frame estimates of instantaneous relative motion [2] can work in constant time, but will inevitably exhibit drift because of accumulation of small errors in the inter-frame motion estimates. Furthermore, from two frames, only the direction of the inter-frame translation can be recovered, not the magnitude. To overcome this difficulty, sets of three or more views are used and the features are triangulated to maintain a consistent scale across the sequence [2], [3]. However, there are also occasional singularities where the epipolar geometry does not fully constrain the motion (e.g. when the camera undergoes a pure rotation).

In this work we aim to retain the advantages of a visual SLAM system, but to incorporate the additional information available from visual odometry style measurements into the filter. In the system described herein, map-to-image matches constrain the scale, as in "standard" monoSLAM. However by taking advantage of the apparent image motion of many features, rather than simply a select few from the map, we improve the accuracy of ego-motion estimation in monoSLAM, both by the effect of noise cancellation from many measurements, and also by overcoming failure-modes of monoSLAM, such as when there are too few map-to-image matches to constrain the ego-motion.

While map-to-image correspondences provide constraints on the absolute position of the camera in the map, two-frame point matches only provide constraints, via the epipolar geometry, on the relative motion of the camera between the two image locations. We show in this paper that such constraints are naturally incorporated into a filter recast from a world-centric frame into a camera-centric frame. To that end we derive the appropriate formulation of robo-centric SLAM [4] for a visual sensor, and show that (as expected) this also yields a more consistent estimate of the filter's uncertainty.

Recently, Civera *et al.* [5] have also presented a monocular SLAM system which uses the robocentric framework and a visual odometry style observations. The observation of all point features is handled by including them as temporary landmarks in a transient map. Once a landmark passes out of view of the camera, it is removed from the map and forgotten. Because of this their system cannot benefit from revisiting a location; even if an old feature is re-observed, it re-enters the map as a new feature. Though they report accurate motion estimates over long sequences (via comparison with GPS data), they do not show a return to the same location,

The authors are with the Department of Engineering Science, University of Oxford, Parks Road, Oxford, United Kingdom bpw,ian@robots.ox.ac.uk. They gratefully acknowledge the financial support of the EPSRC (grant GR/T24685, EP/D037077, and a studentship to BW) and the Royal Society (International Joint Project).

when drift would be apparent. World-centric mapping is impractical in a system with a transient map, so their system is the first to report the use of robo-centric mapping for a visual sensor. Nevertheless they do not report experiments to verify the expected benefits of this framework in terms of filter consistency. Their system is currently unable to achieve real-time operation, requiring about one second to process each frame.

A summary of their objective in that work would be to produce a visual odometry system using the monoSLAM framework. Our aim, in contrast, is to produce a visual SLAM system with a persistent map, but which benefits from visual odometry measurements. To that end, we build on our previous work [6], which was in turn an extension of [1]. Point landmarks are initialised at corner features using the inverse depth parameterisation [7] and are converted when they can be well estimated as a 3D point. At each frame, the system attempts observations of the map landmarks in the image using active search [1] after warping the patch descriptor to match the predicted camera viewing angle. False matches amongst the landmark observations are rejected using the joint compatability branch and bound algorithm [8]. Our key novel contribution is to show how, via the robo-centric framework, we can elegantly incorporate additional measurements from pairwise point matches, as and when possible, and to demonstrate the improved accuracy and consistency that results.

The remainder of the paper is structured as follows. We begin (Section II) by describing our implementation of robot-centric mapping for a single camera SLAM system. The choice of sensor necessitates some differences from the original derivation in Castellanos *et al* [4] though our derivation is very close to Civera's [5]. We then describe how pairwise point matches are expediently utilised to constraint the inter-frame ego-motion (Section III), and then (Section IV) give results on both simulated datasets and real video.

II. ROBOCENTRIC MAPPING

It has been shown that the Extended Kalman Filter suffers from inconsistency due to linearisation errors [9]. After the angular uncertainty grows beyond just a few degrees the filter becomes overconfident and underestimates the uncertainty in the estimates it produces. Castellanos *et al.* [4] have proposed a more consistent SLAM algorithm called robocentric SLAM. In their approach, the state is represented in a frame relative to the current position of the robot. In this frame, the position of the nearby landmarks being observed have lower uncertainty and so the linearisations made are more valid.

More pertinent to our own application is the fact that, because the current pose is always aligned at the origin of the coordinate frame, the new pose is given exactly by the incremental inter-frame motion. This incremental motion is precisely what visual odometry measures. We show in the Section III how these measurements can be incorporated naturally and elegantly, but begin by adapting robocentric mapping [4] to the particularities of a monocular handheld camera.

A. Robocentric State Representation

In the robocentric framework, the state, $\mathbf{x}$, at timestep, k, is parameterised as a multi-dimensional Gaussian represented in the coordinate frame centred on the pose of the camera, C.

$$\mathbf{x}_k \sim \mathcal{N}(\hat{\mathbf{x}}_k^{C_k}, \mathtt{P}_k^{C_k}) \tag{1}$$

where a superscript indicates the reference frame for the estimate.

In the reference frame of the camera, the camera pose is known with certainty and so is not included in the state vector. An entry is created to estimate each map landmark relative to the camera, $\hat{\mathbf{x}}_L^{C_k}$, the linear, $\hat{\mathbf{x}}_v^{C_k}$, and angular velocities, $\hat{\mathbf{x}}_\omega^{C_k}$, of the camera, and the origin and orientation of the world reference frame, $\hat{\mathbf{x}}_W^{C_k}$. This final entry allows the estimate to be transformed into the world representation if required.

B. Prediction and Update Steps

Like the worldcentric approach, the first step in the robocentric EKF is to predict the motion of the camera since the last timestep. Rather than using this motion to recentre the coordinate frame immediately, the incremental motion is instead added to the state vector so that the estimated motion is improved by the update. This helps to reduce the uncertainty and so decrease linearisation error. Our visual odometry observations will greatly improve this motion estimate.

We use a constant velocity motion model to predict this incremental motion. This motion prediction is then placed in the state vector to give the augmented predicted state, $\hat{\mathbf{x}}_{k|k-1}^{C_{k-1}}$. At the same time, the covariance is updated to reflect this prediction.

$$\mathtt{P}_{k|k-1}^{C_{k-1}} = \mathtt{F}_k \mathtt{P}_{k-1}^{C_{k-1}} \mathtt{F}_k^\top + \mathtt{G}_k \mathtt{Q}_k \mathtt{G}_k^\top \tag{2}$$

where

$$\mathtt{F} = \frac{\partial \hat{\mathbf{x}}_{k|k-1}^{C_{k-1}}}{\partial \hat{\mathbf{x}}_{k-1}^{C_{k-1}}} \quad \text{and} \quad \mathtt{G} = \frac{\partial \hat{\mathbf{x}}_{k|k-1}^{C_{k-1}}}{\partial \mathbf{n}} \tag{3}$$

$\mathbf{n}$ is the process noise and $\mathtt{Q}_k$ is covariance.

When using the constant velocity motion model in monocular SLAM, the incremental motion estimate will be correlated with the rest of the state after the prediction stage. This is in contrast to the case of a robot with odometry measurements presented in [4]. The correlations appear in our case because the uncertain velocity estimates in the state vector are used to predict the incremental motion.

The update step in Robocentric Mapping is the same as that of the ordinary EKF, and so is omitted for brevity.

C. Composition Step

The final stage of robocentric mapping is to transform the entire stochastic map so that the new camera pose estimate, $\hat{\mathbf{x}}_k^{C_k}$, is centred at the origin. This is done using the (now refined) incremental motion estimate. The incremental motion and its uncertainty are effectively transferred to the landmark estimates as the motion is marginalised out of the state.

The estimate for each part of the state is calculated through composition with the refined motion

$$\hat{\mathbf{x}}_k^{C_k} = \begin{bmatrix} \ominus \hat{\mathbf{x}}_{C_k}^{C_{k-1}} \oplus \hat{\mathbf{x}}_W^{C_k} \\ \ominus \hat{\mathbf{x}}_{C_k}^{C_{k-1}} \oplus \hat{\mathbf{x}}_v^{C_k} \\ \ominus \hat{\mathbf{x}}_{C_k}^{C_{k-1}} \oplus \hat{\mathbf{x}}_\omega^{C_k} \\ \ominus \hat{\mathbf{x}}_{C_k}^{C_{k-1}} \oplus \hat{\mathbf{x}}_L^{C_k} \end{bmatrix} \tag{4}$$

where $\ominus$ and $\oplus$ are coordinate frame inversion and composition as defined in [4]. The covariance is then transformed using the Jacobian of this transformation, $\mathtt{J}_{C_{k-1}\to C_k}$.

$$\mathtt{P}_k^{C_k} = \mathtt{J}_{C_{k-1}\to C_k} \mathtt{P}_{k|k}^{C_{k-1}} \mathtt{J}_{C_{k-1}\to C_k}^\top. \tag{5}$$

III. VISUAL ODOMETRY

The update time of the EKF algorithm scales quadratically with the number of entries in the state vector. For this reason our system [6], in common with Davison's [1], keeps only a sparse map of landmarks, with typically $10-20$ of these visible at any one time. However this neglects the information available from the image motion of other features. Even without knowledge of the 3D back-projection of an image feature, any pair of matched point features constrains the relative camera motion via the epipolar geometry. Such features are particularly useful in the case that very few map features project into the current frame.

One approach might be to find many matches, solve for the Essential Matrix [10] that encodes the instantaneous epipolar geometry, and then decompose this to yield a translation and rotation. Indeed this is the approach that early visual odometry systems took. We do not take this approach for a number of reasons. First, this method yields only the direction, not magnitude of the translation. Additional non-linear projections would be required to map the result to the state-space of the filter. Second, there exist singularities in which the epipolar geometry is defined, but the decomposition of the essential matrix is underconstrained (such as for a pure rotation of the camera). Third, a minimum of 8 points are required to compute $\mathtt{E}$, but we would like to use additional points expediently, and this may mean using fewer than 8 points on occasion. Finally, in order to fuse the decomposition with the filter estimate would require suitable derivations of the uncertainty in the estimates (tedious, but not impossible).

Instead, we proceed as follows. We begin by determining the predicted Essential Matrix $\hat{\mathtt{E}}$ using the predicted inter-frame motion:

$$\hat{\mathtt{E}} = \left[\hat{\mathbf{t}}_{C_{k|k-1}}^{C_{k-1}}\right]_\times \hat{\mathtt{R}}_{C_{k|k-1}}^{C_{k-1}} \tag{6}$$

where $[.]_\times$ represents the skew symmetric matrix form of the translation.

Each point in frame $k-1$ has a predicted epipolar line in frame k

$$\mathbf{l} = \hat{\mathtt{E}}\mathbf{p}_{k-1} \tag{7}$$

If the prediction were correct, then $\mathbf{p}_k$, the correspondence for $\mathbf{p}_{k-1}$ would lie on this line, up to image noise displacement. In practice, of course, the prediction is wrong, and a Kalman Filter works by applying a correction to the prediction based on the size and covariance of the innovation. Our measurement, then, is the signed (perpendicular) distance of the corresponding point $\mathbf{p}_k$ to the predicted epipolar line. Since the expected measurement is zero, this value is also the innovation.

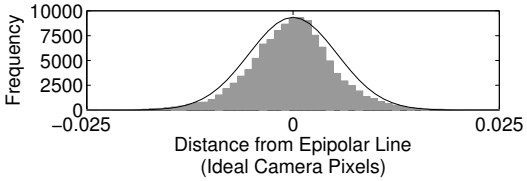

Fig. 1. **Analysis of Visual Odometry Measurements:** The distribution in the innovation for each VO observation in a real sequence conforms to the zero-mean Gaussian assumption in the measurement model.

$$\mathbf{z}_k = \boldsymbol{\nu}_k = \mathbf{p}_k^\top \mathbf{l} \tag{8}$$

(with a suitable normalisation so that $\mathbf{z}$ measures image distance).

The measurement noise, $\mathtt{R}_{VO}$, associated with such measurement is obtained by transforming an estimate of feature localisation accuracy (we use a 1 pixel standard deviation, as is also used for normal map landmark observations), and transforming this via the Jacobians of the image coordinate transformations that are associated with the calibration parameters (mapping image coordinates to ideal coordinates) and inhomogeneous to homogenous coordinate transformation:

$$\mathtt{R}_{VO} = \mathbf{l}_i^\top J_{homog} J_{ideal} \mathtt{R}_{image} J_{ideal}^\top J_{homog}^\top \mathbf{l}_i \tag{9}$$

It is reasonable to ask at this point if the measurements and innovations so obtained are normally distributed, as required by the Kalman Filter. The distribution for measurements for a typical run of the system is shown in Fig. 1, along with a zero-mean Gaussian distribution, which has been fitted to the data. The close fit shown gives us confidence that our assumptions here are valid.

Thus each point-pair match provides us with a one-dimensional measurement which can be fused into the filter just as with any other measurement. Because these features are not added to the map like normal landmarks, we avoid the increased update cost associated with the state vector size ($O(n^2)$).

A. Implementation

As each new frame arrives, we detect corner points in the image using the FAST corner detector [11]. An 11×11 pixel patch around each corner is stored. Then, in the subsequent frame, the image location for each feature is sought using normalised sum-of-squared-difference correlation followed by subpixel refinement [12].

When there are many points, to eliminate outliers we robustly calculate an essential matrix from the matches using the RANSAC method outlined in [13]. The essential matrix calculated here is used only for outlier rejection and plays no further role in the inter frame motion estimation.

B. Example

The visual odometry update is illustrated in Fig. 2 using a simple situation for clarity. The camera begins at the origin looking down the z-axis at 200 points in the world. The camera is then moved backwards and to the right while rotating about the y-axis. Our method is used to correct an inaccurate prediction of the camera motion using the visual odometry measurements of these 200 features. When only visual odometry measurements are used, the estimate for the camera motion after the update matches the true epipolar geometry. However, the estimated motion is correct only up to scale since this is unobservable with only visual odometry measurements. By also including the observation of a single 3D map landmark, this scale is determined and the true motion is estimated correctly.

This is our key innovation in this paper: combining these two observation types allows our system to accurately estimate the motion of the camera while retaining just a sparse map of landmarks to reduce computation time while preventing drift.

IV. RESULTS

To test the performance of the robocentric monocular SLAM system with visual odometry we have run experiments on both real and simulated data. We first test the accuracy of the system by evaluating the performance in simulation. Simulations provide a good test since perfect ground truth is known, and enable us to verify the improved accuracy and consistency claims we make. However, a simulation cannot perfectly replicate realistic operating conditions so a further test of the estimation accuracy is performed using an aerial photo to provide ground truth of the camera position.

A. Estimation Quality in Simulation

The simulation consists of a 100×20 metre courtyard that the camera moves around while facing the wall. The top down view of the map of landmarks and the camera trajectory is shown in Fig. 3. The simulation begins with the camera at the origin with a correct estimate of the initial linear and angular velocities in the state vector. The initial map also contains four known landmarks to fix the scale of the map created.

Twenty Monte Carlo runs were performed using this simulated trajectory. For each run, the monocular SLAM system automatically selected, initialised, and observed landmarks from the simulated environment. Observations of these landmarks were perturbed with random Gaussian Noise with a standard deviation of 0.25 pixels. However, when testing each of the three algorithms on a particular run, the same noisy observations of landmarks were used. Correct data association for each observation was given to the SLAM system.

For visual odometry observations, the simulator randomly selects 200 features in the image plane to track the motion between each timestep. The depth of these features is initialised to be on wall of the courtyard plus a random offset

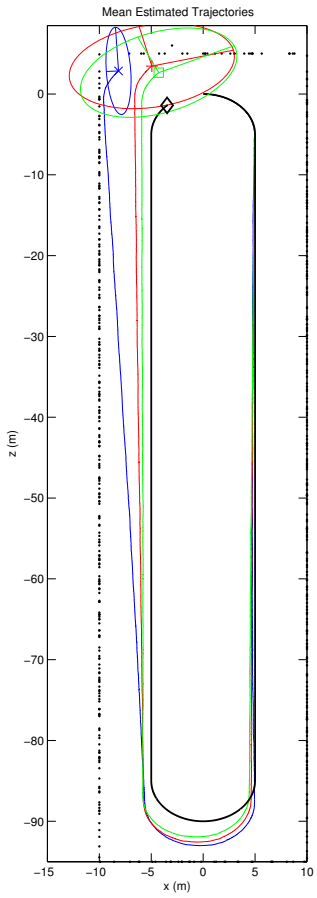

Fig. 3. **Simulation – Mean Estimated Trajectory:** The trajectory used in the simulation is shown in a top down view with the landmarks (●). The camera also followed a 1 metre amplitude sinusoidal motion in the y direction and rocked back and forth about the optical axis $\pm 30°$ to provide a more challenging motion to track. Along with the ground truth (—◇), the mean estimate of 20 Monte Carlo runs is shown for each algorithm, worldcentric (—×), robocentric (—+), and robocentric with visual odometry (—□) with the three standard deviation uncertainty ellipse just before the loop is closed. The robocentric framework produces more consistent estimates and the accuracy is further improved when visual odometry measurements are included. The error in the estimate and uncertainty is analysed for two components of the estimate in Fig. 4.

of up to 2 metres. This offset is used to avoid all of the features lying on a single plane.

The results of these simulated runs can be seen in Fig. 3. Each of the three monocular SLAM techniques is able to track the true pose of the camera throughout the sequence with different degrees of accuracy. The largest part of the error in the estimate for all three techniques is due to scale drift. The perceived scale of the world begins to grow as the camera gets further from the initial known features. This is due to the differences between the assumed motion given by the constant velocity motion model and the true trajectory of the camera. Scale drift is also seen in monocular SLAM when working with real world data. The scale error is corrected when the camera comes around the loop and reobserves the initial features again, 'closing the loop'.

With measurement noise and an imperfect motion model, errors in the estimate are inevitable. However, a good estimation algorithm should keep errors to a minimum and correctly estimate its uncertainty in the answer given. The

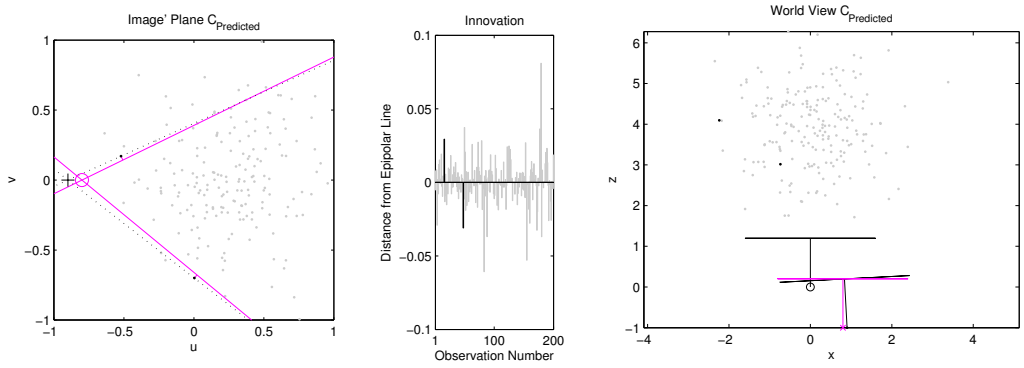

(a) **Before EKF Update:** The predicted motion is incorrect in both translation and rotation leading to an incorrect epipolar geometry prediction.

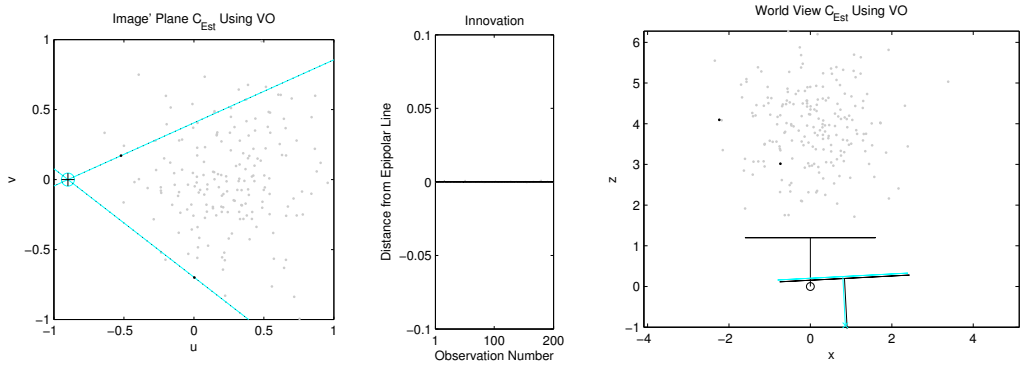

(b) **Updated Using Just Visual Odometry:** The estimated pose is corrected up to a projective ambiguity. With planar motion, the orientation and the direction of the translation is determined but the scale of the translation is not.

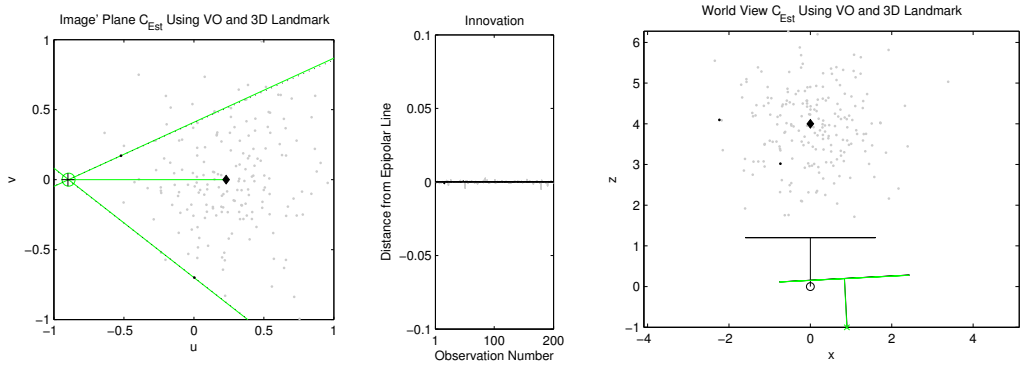

(c) **Updated Using a Landmark and Visual Odometry:** The single measurement of a 3D landmark ♦ removes the projective ambiguity allowing the pose determined.

Fig. 2. **EKF Update Process With Visual Odometry:** This figure illustrates the update process using our proposed visual odometry measurements. The predicted motion estimate (a) is updated using only the visual odometry observations (b) and these observations along with a single 3D map landmark observation (c). *Left Column:* The ideal image plane after motion showing the position of 200 visual odometry features (•), the true (◯) and estimated (+) epipole, and the true (· · ·) and estimated (—) epipolar lines for two selected features (●). *Middle Column:* Perpendicular distance to the epipolar line for each of the visual odometry features given the estimated camera motion. *Right Column:* The 3D pose of camera (⊤) relative to the features (•). The camera starts at the origin and then translates and rotates about the y-axis to the true pose shown in black. The estimate for this pose (×) is in colour.

ideal uncertainty in the estimate is calculated by running the simulation with the same observations but with zero measurement noise. In Fig. 4, a translation and orientation component of the camera pose estimate are examined in detail showing than the robocentric framework provides both a better estimate and a more realistic estimate of the uncertainty.

The underestimation of the uncertainty when using the worldcentric approach is due to linearisation errors. These errors become significant when the orientation uncertainty grows above 2 degrees. Once this occurs, the uncertainty estimate becomes corrupted by linearisation errors and is lower that the ideal uncertainty. This result was also found by Bailey *et al.* [9]. The robocentric approach is able to maintain a better estimate of the uncertainty because in the reference frame of the camera, the angular uncertainty of observed landmarks is much lower.

An estimator is said to be consistent if its state estimation error is unbiased and the actual Mean Square Error matches the calculated covariances. The consistency of an estimation

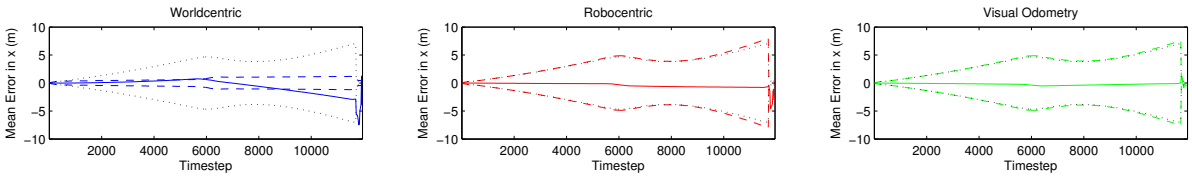

(a) **Position Error (x Coordinate):** The estimate calculated using the worldcentric framework diverges from the ground truth and becomes inconsistent due to linearisation errors. The estimates produced in the robocentric framework stays close to the ground truth and the uncertainty estimate more closely matches the ideal uncertainty.

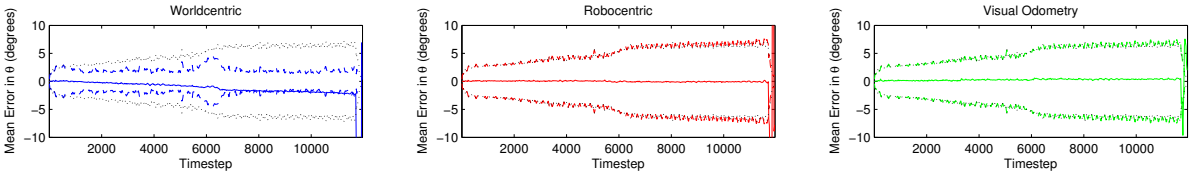

(b) **Angular Error:** θ represents the rotation about the y-axis in Fig. 3. Once the true angular uncertainty grows beyond a couple degrees, linearisation errors cause the uncertainty to be underestimated when the worldcentric framework is used.

Fig. 4. **Estimation Accuracy:** The mean difference (—) between the estimated value and the ground truth for two of the six components of the camera pose was found for 20 Monte Carlo runs. The mean three standard deviation uncertainty (- - -) for the estimate is also shown relative to the ideal uncertainty ($\cdots$) determined using noise-free observations. Without using the robocentric framework, the uncertainty tends to be underestimated once the angular uncertainty grows beyond a couple degrees. Estimates made using the robocentric framework have uncertainty closer to the ideal because linearisation errors are reduced. Consistency results are similar for other translation or orientation components.

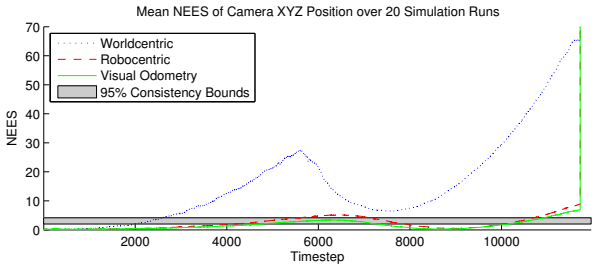

Fig. 5. **Estimation Consistency:** The consistency of the three algorithms is tested by examining the mean normalised estimated error squared (NEES) over twenty Monte Carlo runs in simulation. The 95% consistency bounds are shown in grey.

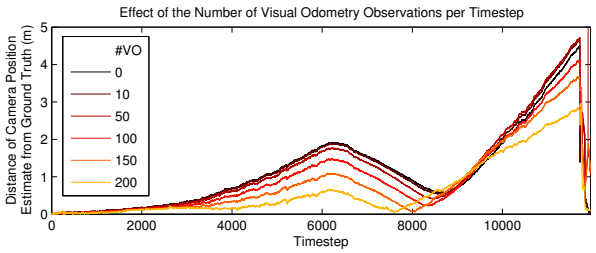

Fig. 6. **Benefit of Visual Odometry Observations:** In this experiment, the number of visual odometry features observed per frame was changed to show the improvement in the estimated camera trajectory compared to the simulation ground truth. Identical noisy landmark observations were used in each run.

algorithm can be investigated by examining the normalised estimation error squared (NEES), ϵ.

$$\epsilon = (\mathbf{x}_k - \hat{\mathbf{x}}_k)^\top (\mathrm{P}_k)^{-1} (\mathbf{x}_k - \hat{\mathbf{x}}_k) \tag{10}$$

If the filter is consistent and linear-Gaussian, ϵ is χ^2 distributed with dimension equal to the size of $\mathbf{x}_k$. Here we perform 20 monte-carlo runs and have calculated the NEES of the camera position estimate. The 95% acceptance region for the χ^2 test is between 2.02 and 4.16. If the average NEES is outside these bounds, it shows the estimator is conservative if lower and optimistic if higher. The results are shown in Fig. 5. More detail on this standard consistency check can be found in [9] and [14].

The simulation also provides a way to test the benefit of visual odometry. The simulation was rerun with different numbers of visual odometry observations but identical noisy landmark observations. Fig. 6 shows that the estimation error generally decreases as the number of visual odometry observations per timestep is increased, as expected.

B. Estimation Quality in the Real World

To test the accuracy of our system on real world data, a sequence was recorded outdoors using a trajectory which can be aligned to an aerial photo. The handheld camera was pointed at a row of buildings while the experimenter walked down the white line painted in the road. This sequence was then used to test the benefit of the robocentric framework and visual odometry measurements. The same landmark observations at each frame were used in each test. The results are shown in Fig. 7. Alignment was performed manually using the trajectory and building facades visible near the start of the trajectory (on the right). This makes any scale drift during the sequence more apparent.

When the traditional worldcentric framework is used, the scale increases over the sequence and the trajectory and map begin to curve towards the top of the image. With the same observations, the robocentric approach gives a very similar final estimate, but with larger estimated uncertainty reflecting a more consistent estimate. When visual odometry measurements are used alongside landmark observations, the motion estimate is far more accurate which in turn leads to a more accurate map estimate. The trajectory can be aligned to match the true trajectory shown by the white line above the parked cars in the photo. We hypothesize that the main benefit here accrues in a few key frames in which only a few map features were observed, and which poorly constrained the motion in the absence of additional VO features.

In another experiment, the accuracy was tested by moving

(a) Worldcentric

(b) Robocentric

(c) Robocentric with Visual Odometry

Fig. 7. **Street Scene:** The camera was moved along the white line just above the parked cars in this aerial photo while facing the buildings. The trajectory estimated using both visual odometry and landmark observations closely matches the true trajectory when aligned with this aerial photo. Without these extra constraints on the motion, the estimate accuracy is worse.

the camera around a loop and then returning to exactly the same position. If the estimated trajectory is correct, the final camera pose estimate will have the same position as the camera position at the start if the sequence. Though, the camera only travelled a relatively small distance in this sequence (3 metres) compared to the outdoor sequence (85 metres), it stayed much closer to the landmarks making this trajectory *effectively* twice as long. This effective distance is determined by noting how many sets of covisible landmarks pass out of view as the camera moves along (9 vs. 5 for the outdoor). All three algorithms were tested using the same observations of landmarks at each frame. At the end of this trajectory, the error in the estimated position for the camera 21cm for the worldcentric algorithm, 16cm for the robocentric, and 13cm for the robocentric with visual odometry. Though our approach produced a more accurate estimate, a separate loop closure detection system would still be needed as the uncertainty at this point is too large to reliably use active search to reobserve the initial landmarks when they come back into view. Several loop closure detection systems for monocular SLAM are discussed in [15].

C. Timing

Due to the computational complexity of the EKF algorithm, the system can only achieve realtime performance (30 Hz) for small maps and small numbers of observations. During all of our experiments here, we allowed the system to make up to 200 visual odometry measurements per frame. The typical cost of matching and performing outlier rejection on this set is *circa* 6ms, or about 20% of the usual per-frame budget.

V. CONCLUSION

We have presented a monocular SLAM system which provides a high quality estimate of the camera pose both in accuracy and consistency. The increase in accuracy is achieved through a novel method for including many more observations per frame without the need of increasing the size of the state estimated. As well as observing the map landmarks at each frame to prevent drift, our system also observes the inter-frame motion of every other corner feature in a visual odometry style method. These extra observations are used to constrain the estimate of the inter-frame motion of the camera leading to a less noisy pose estimate.

The consistency of the estimate is improved through the use of the robocentric mapping framework. We have adapted this technique for use with a handheld camera and have shown that it provides more consistent estimates in monocular SLAM than the traditional worldcentric EKF algorithm. The robocentric framework provides a natural method for handling the visual odometry observations since estimating the inter-frame camera motion at each frame is a key part of the robocentric approach.

REFERENCES

[1] A. Davison, I. Reid, N. Molton, and O. Stasse. MonoSLAM: Real-time single camera SLAM. *IEEE Trans. Pattern Analysis and Machine Intelligence*, 2007.

[2] D. Nistér. An efficient solution to the five-point relative pose problem. *IEEE Trans. Pattern Analysis and Machine Intelligence*, 26(6):756–770, 2004.

[3] D. Nistér, O. Naroditsky, and J. Bergen. Visual odometry for ground vehicle applications. *Journal of Field Robotics*, 23(1), 2006.

[4] J. A. Castellanos, R. Martínez-Cantín, J. D. Tardós, and J. Neira. Robocentric map joining: Improving the consistency of EKF-SLAM. *Robotics and Autonomous Systems*, 55(1):21–29, 2007.

[5] J. Civera, O. Grasa, A. Davison, and J. Montiel. 1-point RANSAC for EKF-based structure from motion. In *Proc. IEEE International Conference on Intelligent Robots and Systems*, 2009.

[6] B. Williams, G. Klein, and I. Reid. Real-time SLAM relocalisation. In *Proc. International Conference on Computer Vision*, 2007.

[7] J. M. M. Montiel, J. Civera, and A. J. Davison. Unified inverse depth parametrization for monocular SLAM. In *Proc. Robotics Science and Systems*, 2006.

[8] J. Neira and J. D. Tardós. Data association in stochastic mapping using the joint compatibility test. In *IEEE Transactions on Robotics and Automation*, pages 890–897, 2001.

[9] T. Bailey, J. Nieto, J. Guivant, M. Stevens, and E. Nebot. Consistency of the EKF-SLAM algorithm. In *Proc. IEEE International Conference on Intelligent Robots and Systems*, 2006.

[10] H. C. Longuet-Higgins. A computer algorithm for reconstructing a scene from two projections. *Nature*, 293:133–135, 1981.

[11] E. Rosten and T. Drummond. Fusing points and lines for high performance tracking. In *Proc. IEEE International Conference on Computer Vision*, pages 1508–1511, 2005.

[12] S. Baker and I. Matthews. Lucas-Kanade 20 years on: A unifying framework. *International Journal of Computer Vision*, 56(3), 2004.

[13] H. Stewénius, C. Engels, and D. Nistér. Recent developments on direct relative orientation. *ISPRS Journal of Photogrammetry and Remote Sensing*, 60:284–294, 2006.

[14] Y. Bar-Shalom, X. R. Li, and T. Kirubarajan. *Estimation with Applications to Tracking and Navigation*. John Wiley and Sons, 2001.

[15] B. Williams, M. Cummins, J. Neira, P. Newman, I. Reid, and J. Tardós. A comparison of loop closing techniques in monocular SLAM. *Robotics and Autonomous Systems*, 2009.